# Fatigue Life Prediction Model for Surface Mountable Power Electronics Fuses

Ramdev Kanapady, Ph.D.
Electronics Division,
Eaton Corporation
Pleasanton, USA
RamdevKanapady@eaton.com

Tissaphern Mirfakhrai, Ph.D.
Electronics Division,
Eaton Corporation
Pleasanton, USA
TissaphernMirfakhrai@Eaton.com

Clarita Knoll
Electronics Division,
Eaton Corporation
Pleasanton, USA
ClaritaKnoll@eaton.com

Zhuomin Liu
Electronics Division,
Eaton Corporation
Pleasanton, USA
ZhuoMinLiu@Eaton.com

***Abstract*—In this paper, a multi-physics based fatigue life prediction model for surface mountable power electronics fuses is presented. It is aimed at a realistic, simple and accurate model development conducted through pulse cycling. Fatigue is the dominating failure mechanism of fuse links and enhancing their cycle life is a major concern for power electronics designers and users. To reduce development time and cost, fatigue life is conventionally obtained empirically through accelerated thermal cycling, which assumes uniform temperature in the fuse link. In actual applications, the fuse assembly is subjected to pulse cycling, power cycling, series of surge currents, etc., and fuse links are subjected to non-uniform temperature. This non-uniform temperature and mismatch of coefficients of thermal expansion (CTE) between fuse components makes the fuse deform differently than the case of uniform temperature. In this work, a pulse cycling analysis scheme is proposed and conducted to predict chip fuse fatigue. Numerical simulations are performed by finite element analyses. It is found that decreasing the cold resistance of the fuse by 38 percent will increase the cycles-to-failure by at least 3x for large ON-times at rated current of wire-in-air fuses.**

***Keywords—Fatigue life, SMD fuses, Wire-in-Air fuses.***

## I. INTRODUCTION

Electronic fuses are designed with an intentional weak link to protect equipment and electrical circuits from overload faults, short-circuit faults and ground faults. Typical ratings of these fuses are 300 volts or below and are used to protect electronic equipment such as power supplies, consumer electronics, and computers. Electronic fuses are classified as either miniature or subminiature type fuses. The subminiature fuse category includes cartridge and surface mount fuses (SMD). A SMD fuse is soldered directly onto a printed circuit board. Standard package sizes for SMD fuses are 0402, 0603, 1206, 6125, and 1025 where for example 0402 size package has a length of 0.04 inches and a width of 0.02 inches. These sizes are standard throughout the electronics industry. Smaller, low profile fuses are highly desired. Smaller fuses also have lower breaking capacity than a larger package size. These package size configurations are compatible with standard pick and place machines used in the PCB industry. Most chip fuses have a fuse element which is deposited onto a ceramic or glass-coated ceramic substrate [1]. Here, we focus on wire-in-air chip fuse geometry description as shown in Fig.1.

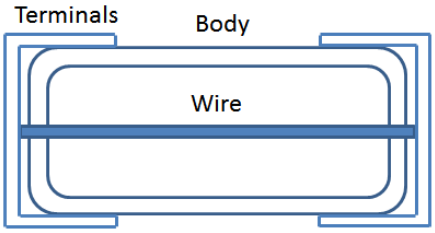


Figure 1: Chip fuse with wire-in-air structure.

The emerging power electronics technologies provide exciting new opportunities, but also create more challenges for engineers aiming to enhance the reliability of electronic products. Emerging technologies, such as vehicle power electronics [2], electric vehicle battery management systems [3, 4], IGBT/MOSFET protection fuses [5], and efficient energy generation, conversion, and storage systems [6]. Nuisance fuse openings are some of the biggest reliability challenges in such applications. These are caused by the fatigue process of crack initiation and growth due to thermal cyclic loads. Thermal cyclic loads are caused by pulse cycling, power cycling, series of surge currents, or thermal cycling due to environmental conditions. Cycles-to-failure prediction models for fuses are proposed by researchers in the past [7-10]. In these previous works, an empirical model based on the fuse cyclic testing [7], a fatigue lifecycle model based on creep model and pulse cyclic test for low current and long ON-time pulses [8] and a fatigue lifecycle model based on finite element analysis (FEA) for thermal cycling of cartridge fuses with a plasticity material model for temperature range of +25 $^{o}$C to +80 $^{o}$C [9] are considered.

For pure copper material, which is used in fuse links, the low temperature creep region can be identified in the deformation mechanism maps [10] as shown in Fig. 2. In this study, FEA based fatigue lifecycle model for pulse cycling of fuse link temperature up to 40% of melting temperature in degree Kelvin (+270 $^{o}$C) for both elastic and plastic regime as indicated by shared region in Fig. 2 is presented. This is for the first time that a full electro-thermo-mechanical multi-physics formulation is proposed to develop the lifecycle model and predict lifetime of the SMD chip fuses.

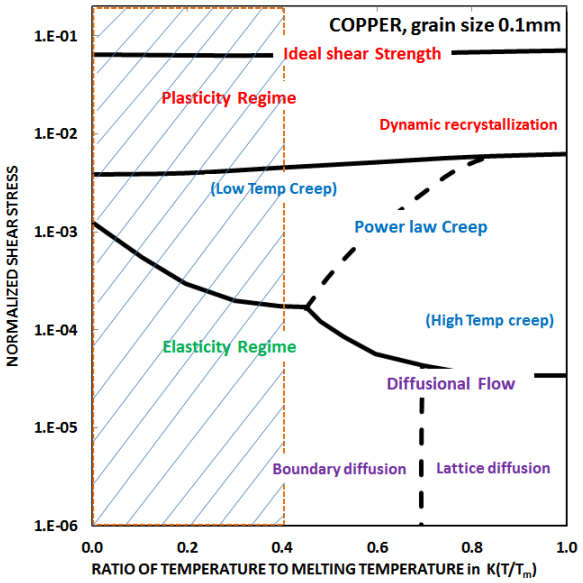


Figure 2: Deformation mechanism map for pure Copper material of grain size 0.1 mm [10].

The organization of this paper is as follows. A brief introduction, motivation and previous work of lifecycle prediction of fuse was described in Section I. Section II presents the governing physics equations pertaining to electrical, thermal, mechanical, and fatigue calculations. Illustrative examples and validations are presented in Section III. Concluding remarks are provided in Section IV.

## II. FUNDAMENTALS OF THE PROPOSED MODEL

It is well known that the stress-strain related to low-cycle fatigue and high-cycle fatigue due to Joule heating and cooling in a fuse links is a very complex phenomenon, which involves the coupled interactions between Joule heating and thermal strain. These thermo-mechanical fatigue cycles cause microstructural material damage to the fuse links, and lead to fatigue crack initiation and propagation, and ultimately to failure. An applied current flowing in an electrically conducting path causes ohmic losses which cause the temperature to rise. This generates heat, which is transported by conduction along the conductor path and dissipated by convection and radiation from the surfaces of the conductors and parts connected to it. This temperature rise additionally causes the ohmic losses to increase due to the increased resistivity of the copper. Moreover, fuse links in actual applications experience non-uniform temperature if the fuse assembly is subjected to pulse cycling, power cycling, series of surge currents, etc. This non-uniform temperature and mismatch of coefficients of thermal expansion (CTE) between fuse components makes the fuse links deform differently than the case of uniform temperature. In the following subsections, governing physics equations and boundary conditions related to electrical, thermal, mechanical, and fatigue calculations for the FEA model are presented. The role of the temperature, which is the key coupling variable between all the three physics, is highlighted.

### A. Joule Heating

Joule heating equation mainly involves following Maxwell's equations Eqs. 1-2 where electric current density $\boldsymbol{j}$ is related to electric field $\boldsymbol{E}$ by $\boldsymbol{j} = \sigma(T)\,\boldsymbol{E}$.

$$\boldsymbol{\nabla} \cdot \boldsymbol{j} = 0 \tag{1}$$

$$\boldsymbol{E} = -\boldsymbol{\nabla} V \tag{2}$$

where $V$ is the voltage, $\sigma(T)$ is electric conductivity which is function of temperature $T$. Figure 3 shows $\sigma(T)$ for copper material considered in this study. The boundary conditions at the ground surface of the fuse assembly is given by

$$V = 0 \tag{3}$$

and the terminal surface of the fuse assembly accounts for the pulse current $I(t)$ is given by Eq. 4.

$$(\boldsymbol{j}.\boldsymbol{n})A = I(t) \tag{4}$$

where $\boldsymbol{n}$ is the unit surface normal, $A$ is the surface area of the terminal available for the current $I(t)$. Above equations are considered only for the conductive part of the fuse assembly.

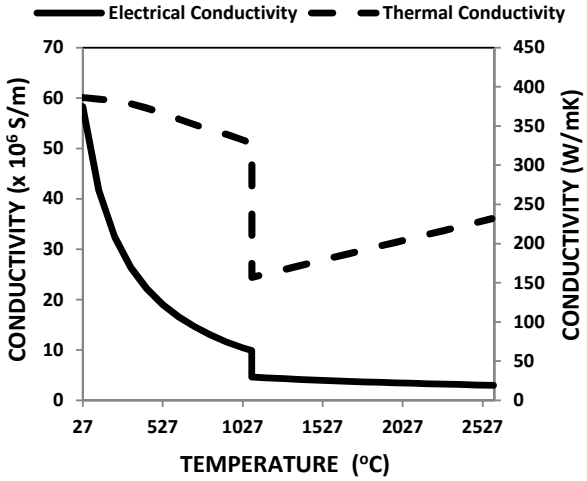


Figure 3: Electrical conductivity ($\sigma$) and thermal conductivity ($k$) of pure Copper material as function of temperature.

### B. Heat Equations

The governing equations for heat energy transport in the fuse assembly are described in Eq. 5

$$\rho(T)C_p(T)\frac{\partial T}{\partial t} + \rho(T)C_p(T)\boldsymbol{v}\cdot\boldsymbol{\nabla}T + \nabla\cdot\boldsymbol{q} = \frac{|\boldsymbol{j}|^2}{\sigma(T)} \tag{5}$$

where $C_p(T)$ is the specific heat at constant pressure and $\rho(T)$ is the material density. Figure 4 shows $C_p(T)$, and Fig. 5 shows $\rho(T)$ for copper material considered in this study. Heat flux $\boldsymbol{q}$ is given by Fourier law in Eq. 6

$$\boldsymbol{q} = -k(T)\boldsymbol{\nabla} T \tag{6}$$

where *k(T)* is the thermal conductivity shown in Fig.3. Boundary conditions of temperature is given by Eq. 7 or heat flux is given by Eq. 8.

$$T = T_0 \tag{7}$$

$$-\boldsymbol{n} \cdot \boldsymbol{q} = q_0 \tag{8}$$

Heat flux $q_0$ can be convective heat flux and/or radiation is given by Eq. 9 from all the surfaces to ambient.

$$q_0 = h(T_{ext} - T); \quad q_0 = \epsilon\sigma(T_{ext}^4 - T^4); \tag{9}$$

Where $\sigma$ is the Boltzmann constant, $\varepsilon$ is the emissivity and $T_{ext}$ is the ambient temperature around the fuse assembly. The current density $\boldsymbol{j}$ in Eq. 5 is the coupling variable for heat source to the thermal model from the electrical equations described in Eqs. 1-2. Unlike in electrical equations, heat equations are considered for the entire fuse assembly of the model. At short-circuit or overload conditions the fuse opens by melting at fuse link weak spots. While pulse cycling is considered for the fatigue life cycle modeling, it is also important to consider modeling the melting condition to avoid thermal runaway due to cycling.

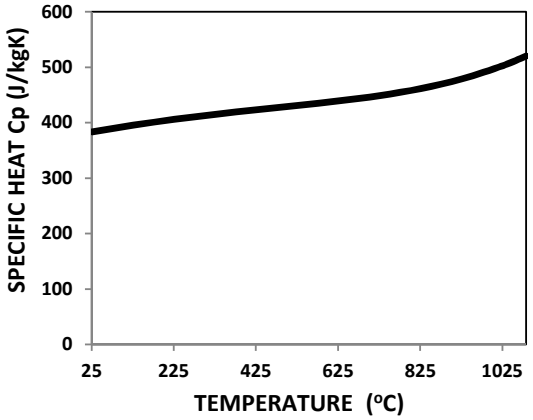


Figure 4: Specific heat ($C_p$) of pure copper material as function of temperature.

During fuse link melting, it is assumed that the phase change occurs over a temperature interval. This temperature interval is assumed to be between $T_{pc} - \Delta T/2$ and $T_{pc} + \Delta T/2$, where $T_{pc}$ is the melting temperature of the copper equal to 1085°C. In this interval, a function, $\theta$, is introduced to represent the fraction of phase before transition with $\theta$ is equal to 1 before $T_{pc} - \Delta T/2$ and 0 after $T_{pc} + \Delta T/2$. The density ($\rho(T)$), the specific enthalpy ($H$) and the thermal conductivity ($k(T)$) are expressed for liquid phase material by Eqs. 10-12.

$$\rho(T) = \theta\rho_{p1}(T) + (1-\theta)\rho_{p2}(T) \tag{10}$$

$$\rho H = \theta\rho_{p1}H_{p1}(T) + (1-\theta)\rho_{p2}H_{p2}(T) \tag{11}$$

$$k = \theta k_{p1}(T) + (1-\theta)k_{p2}(T) \tag{12}$$

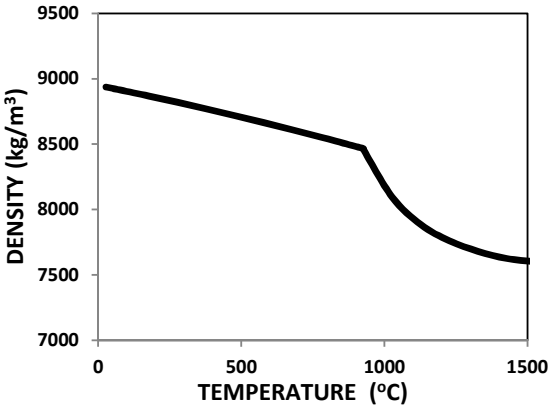


Figure 5: Density ($\rho$) of pure Copper material as function of temperature.

Differentiating the enthalpy Eq. 11 with respect to temperature and after some algebraic manipulations, the effective specific heat for the phase change material can be written as Eq. 13.

$$C_p = \frac{1}{\rho(T)}\big(\theta\,\rho_{p1}(T)C_{p,p1}(T) + (1-\theta)\,\rho_{p2}(T)C_{p,p2}(T)\big) + L\frac{\partial \alpha_m}{\partial T} \tag{13}$$

where $\alpha_m = \frac{(1-\theta)\,\rho_{p1} - \theta\,\rho_{p2}}{\theta\rho_{p1} + (1-\theta)\rho_{p2}}$ and latent heat $L$ is given by

$$L = H_{p1} - H_{p2} \tag{14}$$

Once the temperature history is obtained over a period of time for the pulse current, we need to solve for the stress and the strain at the fuse link. This is described next.

### C. Mechanical Stress-Strains Equations

Governing equations for force balance is given by

$$\nabla \cdot \boldsymbol{s} + \boldsymbol{F}_v = 0 \tag{15}$$

where $\boldsymbol{s}$ is the stress, $\boldsymbol{F}_v$ is the body force and the deformation gradient in the strcuture, $\boldsymbol{F}$, is given by

$$\boldsymbol{F} = \mathbf{I} + \boldsymbol{\nabla u} \tag{16}$$

where $\mathbf{I}$ is the identity matrix, $\boldsymbol{u}$ is the displacement of material in the fuse link. The stress and elastic strain ($\boldsymbol{\epsilon_{el}}$) relationship are defined by constitutive equation

$$\boldsymbol{s} = \boldsymbol{C}(T) : \boldsymbol{\epsilon_{el}} \tag{17}$$

where $\boldsymbol{C(T)}$ is the material tensor function of Young's modulus $E(T)$ which is itself a function of temperature, as illustrated in Fig. 6, and Poisson's ratio. The relationship between total, elastic, and inlastic strains are given by

$$\boldsymbol{\epsilon_{el}} = \boldsymbol{\epsilon} - \boldsymbol{\epsilon_{inel}} \tag{18}$$

$$\boldsymbol{\epsilon_{inel}} = \boldsymbol{\epsilon_0} + \boldsymbol{\epsilon_{th}} + \boldsymbol{\epsilon_{pl}} + \boldsymbol{\epsilon_{cr}} \tag{19}$$

$$\boldsymbol{\epsilon} = \frac{1}{2}[(\nabla \mathbf{u})^{\mathrm{T}} + (\nabla \mathbf{u}) + (\nabla \mathbf{u})^{\mathrm{T}}(\nabla \mathbf{u})] \tag{20}$$

$$\boldsymbol{\epsilon_{th}} = \alpha(T)\big(T - T_{ref}\big)\mathbf{I} \tag{21}$$

where $\boldsymbol{\varepsilon}_{th}$, $\boldsymbol{\varepsilon}_{pl}$, and $\boldsymbol{\varepsilon}_{cr}$ are the thermal, plastic, and creep strains. Creep strain is not considered in this study. $T_{ref}$ is the reference temperature of zero thermal stress and and $\alpha$ is the coefficient of thermal expansion (*CTE*). Figure 7 shows the *CTE(T)* for copper considered in this study. If the fuse link is in contact with any material such as the ceramic body in the case of chip fuse, the difference between the CTEs would govern the deformation and hence the stress and strain in the fuse link. Plastic strains are defined by

$$\dot{\boldsymbol{\epsilon}}_{pl} = \lambda \frac{\partial Q}{\partial \boldsymbol{s}};\ \ \lambda \geq 0;\ \ F\left(\boldsymbol{s}, s_{ys}(T)\right) \leq 0;\ \ \lambda F = 0 \tag{22}$$

where $Q$ is the plastic potential, $\lambda$ is the hardening parameter, $F$ is the yield surface function $S_{ys}(T)$ yield strength of the material which is also function of temperature described for copper in Fig. 6.

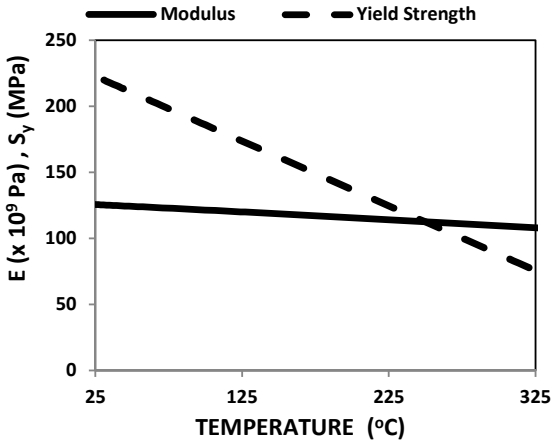


Figure 6: Young's modulus ($E$) and yield strength ($S_y$) as function of temperature for pure copper.

Unlike electrical and thermal equations, the domain of interest for the above mechanical equations can be reduced to include fuse link and components is in contact with the fuse link. The displacement constaint bounadry conditions are considered at the interface where the fuse is soldered to the PCB. The domain of interest for the plasticity equations (Eq. 22) can be restricted to a small region within the fuse link, where the stress levels are above the yield strength of the material. Time-dependent coupled electrical and thermal equations are solved simultaneously for temperature history. Mechanical equations are solved at times where stresses and strains are required to calculate the lifecycles in the fatigue calculations.

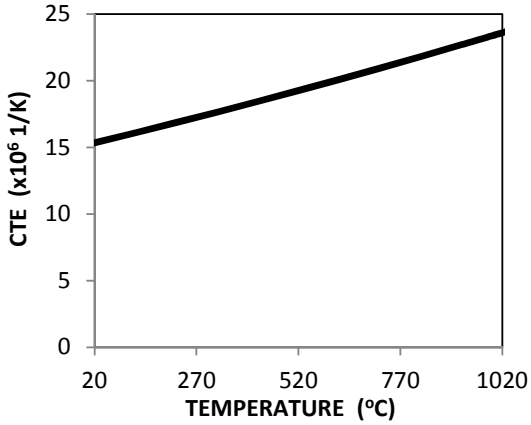


Figure 7: Coefficient of thermal expansion (*CTE*) of pure Copper material as function of temperature.

### *D. Fatigue Calculations*

Once the strains are solved for the peaks and valley temperatures points in the temperature-time history that correspond to the pulse cycle or the power cycle, cycles-to-failure are computed. Predicting the lifecycle of fuse subjected to thermo-mechanical fatigue continues to be a great challenge and there are over one hundred life prediction approaches available [11]. Amongst them, commonly employed approaches are damage summation [12] which accounts for creep damage in addition to inelastic strain, frequency separation [13], strain-range partitioning [14], total strain-range partitioning (TSRP) [15], and strain energy partitioning [16]. Here we employ TSRP method.

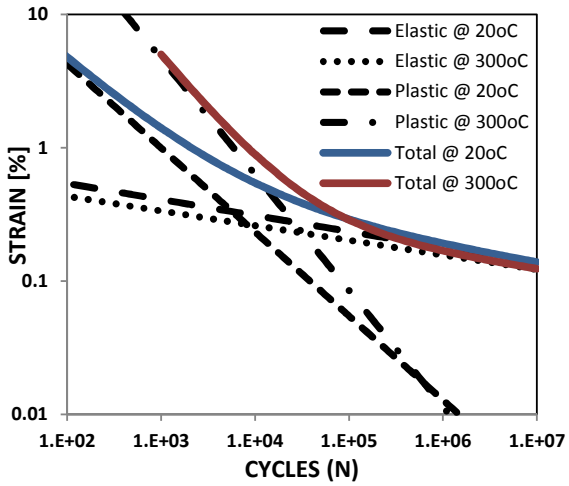


Figure 8: Strain-cycles data for copper from [17] for elastic strain, plastic strain and total strain.

In the TSRP method, the total strain-range is assumed to be the sum of the elastic strain-range and the inelastic strain range and each range can be defined as suggested by Manson-

Coffin theory, so the total strain-range and cycles-to-failure relationship is given as

$$\Delta\epsilon_T = \Delta\epsilon_{el} + \Delta\epsilon_{inel} = B_{el}N_f^{c_{el}} + B_{inel}N_f^{c_{inel}} \qquad (23)$$

where constants $B_{el}$, $C_{el}$, $B_{inel}$ and $C_{inel}$. In this study, copper material strain-cycles data employed is shown in Fig.8 [17] for +20 ºC and +300 ºC. In the case of power cycling, when the current profile is random in nature, then accumulative damage algorithm via the Miner's rule [18,19] is employed.

## III. RESULTS

The developed FEA model is first tested for time-to-melt to validate the electro-thermal model and then for lifecycle model for cycles-to-failure for pulse cycling. Figure 9 shows the test condition of the chip fuse solid model on the test PCB board and Fig. 10 corresponding finite element mesh.

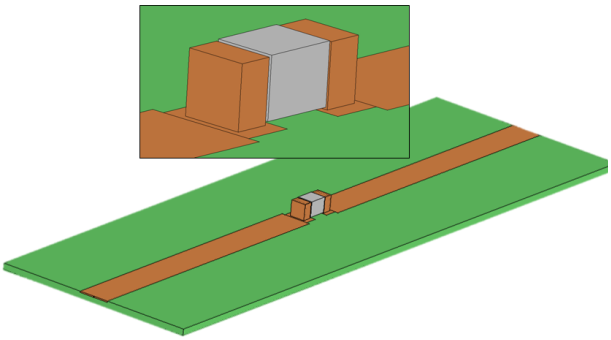

Figure 9: Chip fuse soldered to PCB solid model.

The fuse link is made of copper material. Comsol Multiphysics® FEA software [20] is employed for computing electrical field, temperature field, and stress and strain fields.

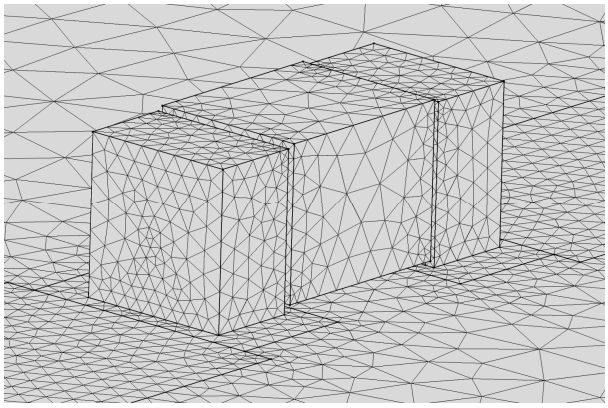

Figure 10: Finite element mesh of the fuse on PCB model.

Figure 11 shows the time-to-melt for various currents for two fuses with cold resistances of 5.5 mΩ and 41.5 mΩ. The simulation results correlates very well with the test results validating the electro-thermal model.

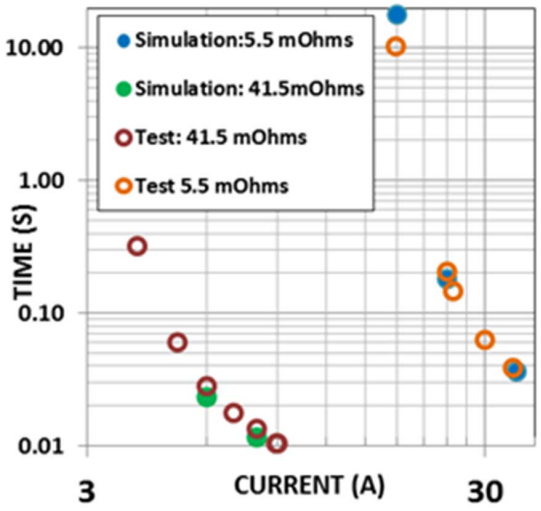


Figure 11: Validation electro-thermal model of the fuse by comparing the model results against test results of time-to-melt of the fuse.

Figure 12 shows cyclic test fixture for pulse current test. Figure 13 shows the cycles-to-failure for two pulses of 2 A and 3 A with different ON-times for 25.5 mΩ and 41.5 mΩ cold resistance fuses. Since these cyclic tests are time consuming there is only one data point to compare against the simulation results, shown in Fig. 12. It should be noted that cycles-to-failure due to fatigue test can have wide scatter (greater than 200 percent [7]). Cycles-to-failure test results show the prediction power of the developed model is quite remarkable. It can be seen that decreasing the cold resistance by 38 percent from 41.5 mΩ to 25.5 mΩ would increase the cycles-to-failure by more than 3 times.

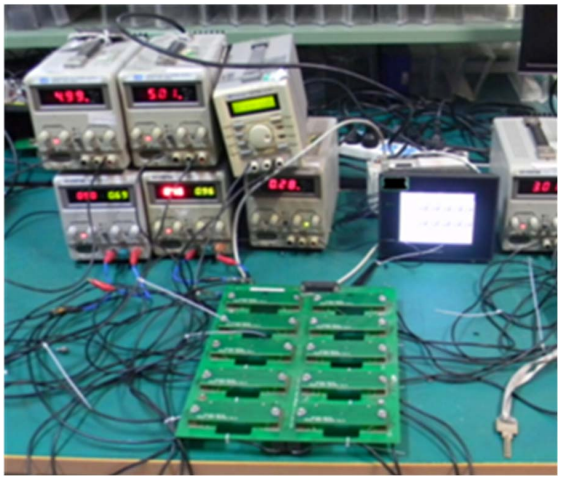

Figure 12: Pulse cyclic test setup with counter to count cycles-to-failure.

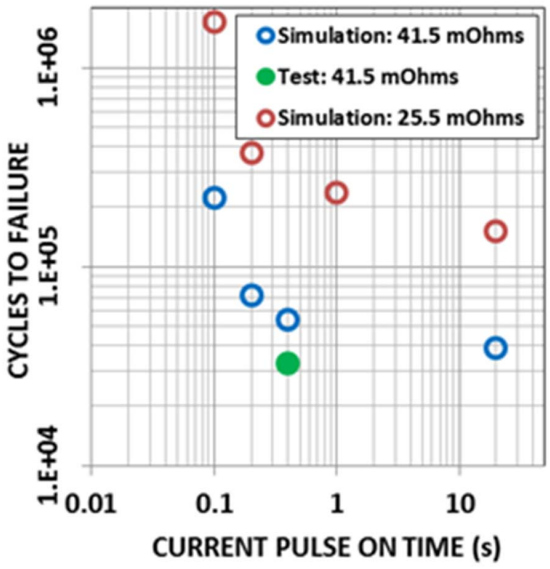


Figure 13: Cycles-to-failure prediction of the fuse for various ON-times for pulse currents.
results of time-to-melt of the fuse

## IV. CONCLUSIONS

In this paper, for the first time, a complete electro-thermo-mechanical multi-physics formulation is proposed to develop the lifecycle model and predict lifetime of the SMD chip fuses. Conventionally, fatigue life is obtained empirically through accelerated thermal cycling, which assumes uniform temperature in the fuse link. In the actual applications, the fuse assembly is subjected to pulse cycling, power cycling, series of surge currents, etc. and fuse links are subjected non-uniform temperature. As our simulations have confirmed, this non-uniform temperature and mismatch of coefficient of thermal expansion between fuse components makes the fuse deform differently from the case of uniform temperature. The predicted time-to-melt results and test results correlate very well, validating electro-thermal model. The predicted cycle-to-failure results correlate remarkably well with the test results. It is found that decreasing the cold resistance by 38 percent will increase the cycles-to-failure by at least 3x for large ON-times of rated current of the wire-in-air fuses.

## REFERENCES


[1] A. Wright and P. G. Newbery, Electric Fuses, Power & Energy Series, 49, The Institution of Engineering and Technology; 3rd edition, 2008.

[2] C. C. Chen and K. T. Chau, An Overview of Power Electronics in Electric Vehicles, IEEE Transactions on Industrial Electronics, Vol 44 (1), February 1997.

[3] M. V. Rajasekhar and P. Gorre, High Voltage Battery Pack Design for Hybrid Electric Vehicles, Transportation Electrification Conference (ITEC), IEEE International, 27-29 Aug. 2015

[4] A. Emadi, Y. J. Lee and K. Rajashekara, Power Electronics and Motor Drives in Electric, Hybrid Electric, and Plug-In Hybrid Electric Vehicles, *IEEE Transactions on Industrial Electronics*, vol. 55, no. 6, pp. 2237-2245, June 2008

[5] W. Puriwatnangkurn, B. Tanboonjit and N. H. Fuengwarodsakul, Overcurrent Protection Scheme of BMS for Li-Ion Battery used in Electric Bicycles, 10th International Conference on Electrical Engineering/Electronics, Computer, Telecommunications and Information Technology (ECTI-CON), 2013.

[6] M. Liserre, T. Sauter and J. Y. Hung, Future Energy Systems: Integrating Renewable Energy Sources into the Smart Power Grid Through Industrial Electronics Selected failure mechanism of modern power modules, *IEEE Industrial Electronics Magazine*, vol. 4, no. 1, pp. 18-37, Mar. 2010.

[7] J. Gelet, Thermal Fatigue of Electrical Fuses. MATEC Web of Conferences, 2, 2014.

[8] X. Z. Meng and J. G. J. Sloot, Reliability Concept for Electric Fuses, IEEE Proc.-Sci. Meas. Technol., vol 144 (2), March 1997.

[9] A. S. Bahman, F. Iannuzo and F. Blaabjerg, Fuse Modeling for Reliability Study of Power Electronics Circuits, Applied Power Electronics Conference and Exposition (APEC), 26-30 March 2017 IEEE.

[10] H. J. Frost and M. F. Ashby, Deformation-Mechanism Maps, The Plasticity and Creep of Metals and Ceramics, Pergamon Press, 1982.

[11] G. Halford, Brief Summary of the Evolution of High-Temperature Creep-Fatigue Life Prediction Models for Crack Initiation, NASA-CP-3230, 1993.

[12] S. Taira, Lifetime of Structures Subjected to Varying Load and Temperature, Creep in Structures, N., J., Hoff (ed.), SPRINGER-VERLAG, pp. 96-124, 1962.

[13] L. Jr. Coffin, The Concept of Frequency Separation in Life Prediction for Time-Dependent Fatigue, in 1976 ASME-MPC Symposium on Creep-Fatigue Interaction, MPC-3, American Society for Mechanical Engineers, New York, pp. 349-364, 1976.

[14] S. Manson, G. Halford, and M. Hirschberg, Creep-Fatigue Analysis by Strain Range Partitioning, Symposium on Design for Elevated Temperature Environment, ASME, New York, pp. 12-28, 1971.

[15] G. Halford and J. Saltsman, Strain Range Partitioning - A Total Strain Range Version, Advances in Life Prediction Methods, D. A. Woodford and J. R. Whitehead, eds., ASME, New York, pp. 17-26. 1983.

[16] J. He, Z. Duan, Y. Ning and D. Zhao, Strain Energy Partitioning and its Application to GH33A Nickel-base Super Alloy and 1Cr-18Ni-9Ti Stainless Steel, Proceedings of ASME international conference on advances in life prediction methods, New York, pp27-32, April 1983.

[17] P. Agostinetti, S. D. Belloa, M. D. Palma, B. Heinemann, R. Nocentini, C. Zauner, H. Langer and J. Klammer, Investigation of the Thermo-mechanical Properties of Electro-deposited Copper for ITER, Journal of Nuclear Materials, Volume 417, pp, 925-927, October 2011.

[18] V. Rathod, O. P. Yadav, A. Rathore, and R. Jain, Probabilistic Modeling of Fatigue Damage Accumulation for Reliability Prediction, International Journal of Quality, Statistics, and Reliability, vol 2011, Article ID 718901.

[19] R. Kanapady, K. Y. Kyle, and J. Lee, Battery Life Estimation Model and Analysis for Electric Buses with Auxiliary Energy Storage Systems, Thirty Second Annual IEEE Appl. Power Electron. Conference, pp. 945–950, 2017.

[20] COMSOL Multiphysics® version 5.3, www.comsol.com